Electronic version of paper:
Rieckh, G., Kreuzer, W., Waubke, H. and Balazs P.: A 2.5D-Fourier-BEM-model for vibrations in a tunnel running through layered anisotropic soil, in: Engn. Anal. Bound. Elem. 36, 960–967, (2012)
doi: http://dx.doi.org/10.1016/j.enganabound.2011.12.014

A 2.5D-Fourier-BEM model for vibrations in a tunnel running through layered anisotropic soil

Georg Rieckh[1,2,*], Wolfgang Kreuzer[1], Holger Waubke[1], and Peter Balazs[1]

[1]Austrian Academy of Sciences, Acoustics Research Institute, Wohllebengasse 12-14, 1040 Vienna, Austria
[2]IST Austria (Institute of Science and Technology Austria), Am Campus 1, 3400 Klosterneuburg, Austria
[*]Corresponding author: georg.rieckh@oeaw.ac.at

December 21, 2011

Abstract

A boundary element model of a tunnel running through horizontally layered soil with anisotropic material properties is presented. Since there is no analytical fundamental solution for wave propagation inside a layered orthotropic medium in 3D, the fundamental displacements and stresses have to be calculated numerically. In our model this is done in the Fourier domain with respect to space and time. The assumption of a straight tunnel with infinite extension in the x direction makes it possible to decouple the system for every wave number k_x, leading to a 2.5D-problem, which is suited for parallel computation. The special form of the fundamental solution, resulting from our Fourier ansatz, and the fact, that the calculation of the boundary integral equation is performed in the Fourier domain, enhances the stability and efficiency of the numerical calculations.

1 Introduction

With the increase of heavy traffic and the construction of rail-road tracks in or close to residential areas, it is more and more important to have numerical models to predict vibrations caused by construction work and transportation, since they might compromise quality of life and effect sensitive equipment (e.g. in hospitals). For isotropic materials a wide range of numerical methods is used, e.g. finite difference methods [1, 2], finite element methods [3, 4], boundary element methods [5, 6, 7, 8, 9] or combinations of these methods [10, 11, 12, 13].

Since the boundary element method (BEM) has certain advantages when dealing with unbounded domains [14], and soil can be modeled as an infinite half space, the BEM is a good choice for simulating wave propagation in such a medium. The simplest generalization of isotropy is transverse orthotropy, which can be used to model rock masses [15]. The method presented here also works for general anisotropy. However, we restricted the approach to transverse

orthotropy to keep calculations simple and the number of input parameters small. The soil is modeled as a horizontally layered half space to account for different strata. However, for this kind of media no analytical fundamental solution, which is essential for the boundary element method, is available.

In the literature on the fundamental solution for (layered) anisotropic media approaches using the Fourier transformation can be found quite frequently [16, 17, 18, 19, 20, 21, 22, 23, 24, 25, 26]. They have the advantage, that the infinite point load (represented by the Dirac delta distribution) used in the definition of the fundamental solution is transformed into a finite quantity [27], i.e. a bounded function. The constructed fundamental solution is then transformed back into the regular domain and the boundary integral equation (BIE) can be solved using standard techniques. However, this approach induces certain numerical problems, because the integrands of the BIE contain singularities caused by the fundamental solution. If the BIE is solved numerically in the regular domain, a lot of quadrature points are needed around these singularities. This makes a numerical inverse transformation rather inefficient.

In our new approach, the approximation of the fundamental solution is constructed in the semi-Fourier domain (k_x, k_y, z), i.e. the function is given on a discrete grid in the horizontal Fourier domain (k_x, k_y), whereas in the z direction the solution can be given analytically. The integrals over the boundary elements and the one resulting from the inverse Fourier transformation are exchanged, which has the advantage, that an integration over the singularity of the fundamental solution can be avoided. The integral with respect to the depth z can be solved analytically, and the integral with respect to k_x and k_y (the inverse Fourier transformation) can be solved with simple quadrature schemes.

This paper is structured as follows. In Section 2 we introduce the geometric properties of our model. The BEM-formulation to model a tunnel excited by a vibrating load on the tunnel base, will be described in Section 3. Using properties of the Fourier transformation, the BIE can be decoupled for every wave number k_x [28]; thus it is possible to treat the 3D problem as a set of smaller 2D problems (in the literature this is sometimes called 2.5D [29, 30, 31, 32, 33]), which reduces its overall complexity. A way to construct a numerical approximation of the fundamental solution for wave propagation in a layered, transversely orthotropic medium is presented in Section 4. Results from this section are then used to numerically solve the boundary integral equation in Section 5. Finally, Section 6 gives some results for a test example.

2 Geometric setup

In our model, the soil is assumed to be a horizontally layered orthotropic half space. The material parameters in each layer are given by the Young's moduli $E_x^{(l)}$ and $E_z^{(l)}$, the shear moduli $G_{xy}^{(l)}$ and $G_{zx}^{(l)}$, the Poisson ratios $\nu_{xy}^{(l)}$ and $\nu_{zx}^{(l)}$, density $\rho^{(l)}$ and thickness $d^{(l)}$, where l is the number of the layer. Underneath the last layer, a half space with appropriate boundary conditions is added to prevent (unwanted) reflections at the bottom [34, 4].

In this layered half space, we assume a tunnel (see Fig. 1), which has infinite straight extension in the x direction and a closed cross section of finite area. The model will be used to calculate vibrations at the tunnel walls, the tunnel base, certain evaluation points in the ground and at the soil surface, caused by

a vibrating load at the tunnel base.

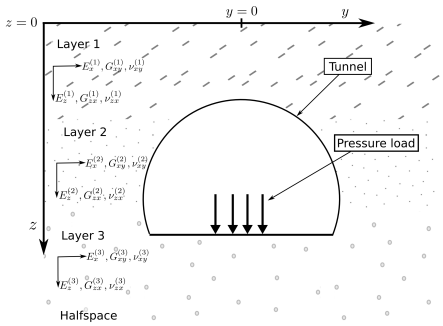

Figure 1: Cross section of the model. In this example the soil consists of three regular layers and a final half space layer. The pressure load is applied at the tunnel base. The positive z direction is pointing downwards.

3 Boundary integral formulation of the model

As governing equation, the body-force free Somigliana's identity [14, 35] is used:

$$u_i(\boldsymbol{\xi}) = \int_\Gamma \sum_j u^*_{ij}(\boldsymbol{\xi}, \boldsymbol{x}) t_j(\boldsymbol{x}) \; d\boldsymbol{x} - \int_\Gamma \sum_j t^*_{ij}(\boldsymbol{\xi}, \boldsymbol{x}) u_j(\boldsymbol{x}) \; d\boldsymbol{x} \; , \tag{1}$$

or in a matrix/vector-notation

$$\boldsymbol{u}(\boldsymbol{\xi}) = \int_\Gamma \boldsymbol{U}^*(\boldsymbol{\xi}, \boldsymbol{x}) \boldsymbol{t}(\boldsymbol{x}) \; d\boldsymbol{x} - \int_\Gamma \boldsymbol{T}^*(\boldsymbol{\xi}, \boldsymbol{x}) \boldsymbol{u}(\boldsymbol{x}) \; d\boldsymbol{x} \; , \tag{2}$$

where $\boldsymbol{u} = (u_x, u_y, u_z)^T$ is the vector of displacements in the x, y, and z direction, and $\boldsymbol{t}$ is the vector containing the tractions $t_i(\boldsymbol{x}) = \sum_j \sigma_{ij} n_j$, where $\mathbf{n} = (0, -\sin(\alpha), -\cos(\alpha))^T$ is the vector normal to the tunnel surface Γ and α the inclination of the tunnel wall (see Fig. (2)). Please note, that because of the assumption of a straight tunnel in the x direction, $\mathbf{n}$ is not dependent on x. Furthermore $[\boldsymbol{U}^*(\boldsymbol{\xi}, \boldsymbol{x})]_{ij} = u^*_{ij}(\boldsymbol{\xi}, \boldsymbol{x})$ is given by the fundamental displacements in j directions at the evaluation point $\boldsymbol{x} = (x, y, z)$ caused by a load applied at $\boldsymbol{\xi} = (\xi, \eta, \zeta)$ in the i direction (we use a slightly inexact notation insofar as x, y and z signify *both*, the three spatial directions, *and* the coordinates of a point $\boldsymbol{x}$, but the meaning should always be clear from the context). The t^*_{ij} are the fundamental stresses normal to the tunnel boundary Γ (fundamental tractions) and are defined as follows:

$$t^*_{ij}(\boldsymbol{\xi}, \boldsymbol{x}) := \sum_k \sigma^*_{ijk}(\boldsymbol{\xi}, \boldsymbol{x}) n_k(\boldsymbol{x}) \; , \tag{3}$$

where $\sigma^*_{ijk}(\boldsymbol{\xi}, \boldsymbol{x})$ is the jk-component of the stress tensor at $\boldsymbol{x}$ caused by a unit load in the i direction at the point $\boldsymbol{\xi}$. On the surface of the tunnel Neumann like boundary conditions are used, i.e. the tractions $\boldsymbol{t}(\boldsymbol{x}) = \mathbf{0}$ on Γ, except at the tunnel base, where the vibrating load is applied (see Fig. 2).

Note that although $\boldsymbol{u}^*(\boldsymbol{\xi}, \boldsymbol{x})$ is shift invariant in the x and y direction, shift invariance with respect to z is not given, because of the different material layers. i.e.

$$\boldsymbol{u}^*(\boldsymbol{\xi}, \boldsymbol{x}) = \boldsymbol{u}^*(\xi, \eta, \zeta\,;\, x, y, z) = \boldsymbol{u}^*(0, 0, \zeta\,;\, x-\xi, y-\eta, z)\ . \tag{4}$$

Corresponding statements hold for the fundamental stresses.

3.1 Decoupling of the 3D-problem into a set of 2D-problems

Since the tunnel is assumed to have infinite extension in the x direction, Eq. (2) can be rewritten as

$$\begin{aligned}\boldsymbol{u}(\xi, \eta, \zeta) + \int_{\Gamma'} \int_{-\infty}^{\infty} \boldsymbol{T}^*(\xi, \eta, \zeta; x, y, z)\boldsymbol{u}(x, y, z)\ dx\ d\Gamma' - \\ - \int_{\Gamma'} \int_{-\infty}^{\infty} \boldsymbol{U}^*(\xi, \eta, \zeta; x, y, z)\boldsymbol{t}(x, y, z)\ dx\ d\Gamma' = \boldsymbol{0}\ ,\end{aligned} \tag{5}$$

where Γ' is the boundary of the cross section of the tunnel in the (y, z)-plane (just called 'cross section' from now on).

In the following, we will only focus on the integrals with respect to x. To simplify notation, the dependencies on y, z, η and ζ will be dropped for the moment. Using the shift invariance with respect to x and shortening the notation, we can reformulate Eq. (5):

$$\begin{aligned}\boldsymbol{u}(\xi) + \int_{\Gamma'} \int_{-\infty}^{\infty} \boldsymbol{T}^*(x-\xi)\boldsymbol{u}(x)\ dx\ d\Gamma' - \\ - \int_{\Gamma'} \int_{-\infty}^{\infty} \boldsymbol{U}^*(x-\xi)\boldsymbol{t}(x)\ dx\ d\Gamma' = \boldsymbol{0}\ .\end{aligned} \tag{6}$$

After a one-dimensional Fourier transformation and the use of the convolution theorem (see Eq. (42)), Eq. (6) becomes

$$\begin{aligned}\breve{\boldsymbol{u}}(k_x) + \int_{\Gamma'} \breve{\boldsymbol{T}}^*(-k_x)\breve{\boldsymbol{u}}(k_x)\ d\Gamma' - \\ - \int_{\Gamma'} \breve{\boldsymbol{U}}^*(-k_x)\breve{\boldsymbol{t}}(k_x)\ d\Gamma' = \boldsymbol{0}\ ,\end{aligned} \tag{7}$$

where $\breve{\cdot}$ denotes the Fourier transform with respect to x.

It is therefore possible to consider the BIE separately for every wavenumber k_x, thus reducing the integrals in Eq. (2) to simple curve integrals over the tunnels cross section Γ'. Consequently, we have reduced the 3D problem to a set of independent 2D problems and it is only necessary to discretize the cross section of the tunnel - and not the whole tunnel - with a mesh. This fact can be used for an efficient implementation of the model using parallel computation, because every thread can work independently with a different value of k_x. Please note, that although the integrals have been reduced to 2D, still the fundamental solutions for the 3D-space have to be used.

3.2 Transformation to linear system

To transform the boundary integral equation into a linear system, the collocation method is used. The BEM-mesh of the cross section $\Gamma' = \bigcup_{p=1}^{N} \Gamma'_p$ consists of constant line elements Γ'_p (see Fig. 2) with one collocation node (y_p, z_p) in the middle of the element. The linear system is then given as

$$\mathbf{M}\breve{\mathbf{u}} = \breve{\mathbf{f}} \ , \tag{8}$$

where $\mathbf{M}$ is a block matrix with 3×3 blocks $\mathbf{M}_{pq}$, which are given by

$$\mathbf{M}_{pq} = \frac{\delta_{pq}}{2}\mathbf{I}_3 + \int_{\Gamma'_q} \breve{\boldsymbol{T}}^*(y_p, z_p; y, z) \ d\Gamma'_q \ , \tag{9}$$

where $\mathbf{I}_3$ denotes the 3×3 unit matrix, δ_{pq} denotes the Kronecker delta and $p, q = 1, \ldots, N$. $\breve{\mathbf{u}}$ is a vector containing the nodal displacements in all three directions

$$\breve{\mathbf{u}}_q = \breve{\boldsymbol{u}}(y_q, z_q) \tag{10}$$

and $\mathbf{f}$ is given by

$$\mathbf{f}_p = \left(\int_{\Gamma'_q} \breve{\boldsymbol{U}}^*(y_p, z_p; y, z) \ d\Gamma'_q \right) \breve{\boldsymbol{t}}(y_q, z_q) \ . \tag{11}$$

For easier implementation we made the minor restriction, that every element is fully contained within one material layer.

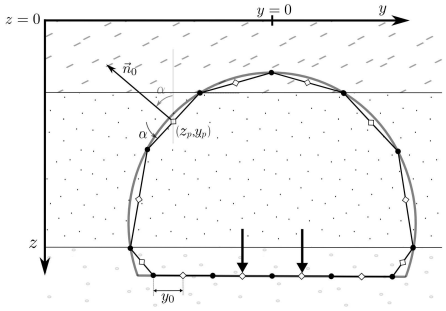

Figure 2: Scheme of the tunnel cross section and its discretization. The outside normal vector is $(0, -\cos(\alpha), -\sin(\alpha))^T$.

4 Construction of the fundamental solution

The fundamental solution can be seen as the response of a system at a field point $\boldsymbol{x}$ to an (infinitely large) point load applied at a load point $\boldsymbol{\xi}$, described by the Dirac delta functional $\delta(\boldsymbol{\xi})$. With the Fourier transformation this δ-load is transformed into a finite quantity, which makes it possible to numerically calculate the fundamental displacements $\hat{\boldsymbol{u}}^*$ in the Fourier domain for given pairs of load and field point.

As a first step, we are looking at the problem of wave propagation in one single layer.

4.1 Fundamental solution for a single layer

The problem of wave propagation inside one homogeneous layer is governed by $\sum_j \sigma_{ij,j} - \rho\frac{\partial^2}{\partial t^2}u_i + b_i = 0$ $(i,j \in \{x,y,z\})$, where the index after the comma indicates partial derivation. After a Fourier transformation with respect to time t, the main equation becomes:

$$\begin{pmatrix} \frac{\partial\sigma_{xx}}{\partial x} + \frac{\partial\sigma_{xy}}{\partial y} + \frac{\partial\sigma_{xz}}{\partial z} \\ \frac{\partial\sigma_{xy}}{\partial x} + \frac{\partial\sigma_{yy}}{\partial y} + \frac{\partial\sigma_{yz}}{\partial z} \\ \frac{\partial\sigma_{xz}}{\partial x} + \frac{\partial\sigma_{yz}}{\partial y} + \frac{\partial\sigma_{zz}}{\partial z} \end{pmatrix} + \rho\omega^2 \begin{pmatrix} u_x \\ u_y \\ u_z \end{pmatrix} + \begin{pmatrix} b_x \\ b_y \\ b_z \end{pmatrix} = \begin{pmatrix} 0 \\ 0 \\ 0 \end{pmatrix} , \tag{12}$$

where u_x, u_y, u_z are the unknown displacements in the x, y and z directions, σ_{ij} $(i,j \in \{x,y,z\})$ are the components of the stress tensor, ρ is the density of the material, ω the angular frequency to be considered and b_x, b_y and b_z are external body forces in the x, y and z direction.

The relation between the stresses $\boldsymbol{\sigma} = (\sigma_{xx}, \sigma_{yy}, \sigma_{zz}, \sigma_{yz}, \sigma_{xz}, \sigma_{xy})^T$ and the displacements $\boldsymbol{u} = (u_x, u_y, u_z)^T$ is given by

$$\boldsymbol{\sigma} = \boldsymbol{F}^{-1}\boldsymbol{D}\boldsymbol{u} , \tag{13}$$

where $\boldsymbol{F}$ is the stiffness matrix for transverse orthotropic media and

$$\boldsymbol{D} = \begin{pmatrix} \frac{\partial}{\partial x} & 0 & 0 \\ 0 & \frac{\partial}{\partial y} & 0 \\ 0 & 0 & \frac{\partial}{\partial z} \\ 0 & \frac{\partial}{2\partial z} & \frac{\partial}{2\partial y} \\ \frac{\partial}{2\partial z} & 0 & \frac{\partial}{2\partial x} \\ \frac{\partial}{2\partial y} & \frac{\partial}{2\partial x} & 0 \end{pmatrix} . \tag{14}$$

Setting the body forces b_i in Eq. (12) to zero (i.e. assuming free wave propagation inside the layer), and applying the three-dimensional Fourier transformation with respect to x, y and z, transforms Eq. (12) into the system of algebraic equations

$$\begin{pmatrix} \mathrm{i}k_x\tilde{\sigma}_{xx} + \mathrm{i}k_y\tilde{\sigma}_{xy} + \mathrm{i}k_z\tilde{\sigma}_{xz} \\ \mathrm{i}k_x\tilde{\sigma}_{xy} + \mathrm{i}k_y\tilde{\sigma}_{yy} + \mathrm{i}k_z\tilde{\sigma}_{yz} \\ \mathrm{i}k_x\tilde{\sigma}_{xz} + \mathrm{i}k_y\tilde{\sigma}_{yz} + \mathrm{i}k_z\tilde{\sigma}_{zz} \end{pmatrix} + \rho\omega^2 \begin{pmatrix} \tilde{u}_x \\ \tilde{u}_y \\ \tilde{u}_z \end{pmatrix} = \begin{pmatrix} 0 \\ 0 \\ 0 \end{pmatrix} , \tag{15}$$

where $\tilde{\boldsymbol{\sigma}}$ and $\tilde{\boldsymbol{u}}$ denote the Fourier transforms (with respect to all coordinates) of $\boldsymbol{\sigma}$ and $\boldsymbol{u}$ respectively, and $\mathrm{i}^2 = -1$.

In the Fourier domain, the stresses can be expressed as a linear combination of the displacements (see also Eq. (13)), thus Eq. (15) is transformed into a linear system of equations:

$$\boldsymbol{A}\tilde{\boldsymbol{u}} = \boldsymbol{0} , \tag{16}$$

where the symmetric 3×3 matrix $\boldsymbol{A}$ depends on the material parameters of the layer, the wave numbers k_x, k_y and k_z, and the angular frequency ω. For the actual coefficients of $\boldsymbol{A}$, please refer to B.

A nontrivial solution of Eq. (16) only exists iff $\boldsymbol{A}$ is singular, i.e. iff $\det(\boldsymbol{A}) = 0$. The determinant of $\boldsymbol{A}$, viewed as a function of k_z, is a polynomial of degree 6

(see the matrix entries in B). Consequently, for fixed values of (k_x, k_y, ω) at most 6 different values $k_z^{[j]}$ $(j = 1, \ldots, 6)$ exist, for which Eq. (16) has a nontrivial solution.

The $k_z^{[j]}$ can be seen as eigenvalues of a quadratic eigenvalue problem [36], that can be obtained by reformulating Eq. (16). Therefore, in the remainder of this article, we shall call them *eigenvalues*, the corresponding vectors $\boldsymbol{\Psi}^{[j]}(k_x, k_y) \in \ker \boldsymbol{A}(k_x, k_y, k_z^{[j]})$ will be the *eigenvectors* of the system and an ordered pair $(k_z^{[j]}, \boldsymbol{\Psi}^{[j]})$ will be an *eigenpair* iff $\boldsymbol{A}(k_x, k_y, k_z^{[j]}, \omega)\boldsymbol{\Psi}^{[j]} = \boldsymbol{0}$. By looking at the entries of $\boldsymbol{A}$, it can easily be seen, that if $(k_z^{[j]}, \boldsymbol{\Psi}^{[j]})$ is an eigenpair, $(-k_z^{[j]}, \boldsymbol{S}_3\boldsymbol{\Psi}^{[j]})$ is also an eigenpair, where $\boldsymbol{S}_3 = \mathrm{diag}(1, 1, -1)$. Also, if $\boldsymbol{\Psi} = (\Psi_x, \Psi_y, \Psi_z)^T$ is an eigenvector for $\boldsymbol{A}(k_x, k_y, k_z^{[j]})$, then $(-\Psi_x, \Psi_y, \Psi_z)^T$ is an eigenvector for $\boldsymbol{A}(-k_x, k_y, k_z^{[j]})$.

After a discretization of the (k_x, k_y) plane, the eigenvalues for the given angular frequency ω are calculated using the fact, that $\det(\boldsymbol{A}(k_z))$ can be reduced to a polynomial of degree 3 (as a function of k_z^2) and thus Cardano's method to solve cubic equations can be applied. The eigenvectors can then be calculated directly, since the matrices involved are small.

Every solution of Eq. (16) can be written as a linear combination of eigenpairs:

$$\tilde{\boldsymbol{u}}(k_x, k_y, k_z) = \sum_{j=1}^{6} a_j \boldsymbol{\Psi}^{[j]}(k_x, k_y)\delta(k_z - k_z^{[j]}) \ , \tag{17}$$

or after an inverse transformation with respect to k_z:

$$\hat{\boldsymbol{u}}(k_x, k_y, z) = \frac{1}{2\pi} \sum_{j=1}^{6} a_j \boldsymbol{\Psi}^{[j]}(k_x, k_y) e^{\mathrm{i}k_z^{[j]} z} \ . \tag{18}$$

This can be seen as an analogue to the Helmholtz potentials in the isotropic case. Note that the tilde $(\tilde{\cdot})$ denotes entities in the (k_x, k_y, k_z)-domain, whereas the hat $(\hat{\cdot})$ is related to the (k_x, k_y, z)-domain.

The Fourier transformed version of Eq. (13) reads

$$\tilde{\boldsymbol{\sigma}} = \boldsymbol{F}^{-1}\tilde{\boldsymbol{D}}\tilde{\boldsymbol{u}} \ , \tag{19}$$

where the stiffness matrix $\boldsymbol{F}$ contains only constants and due to the linearity of the Fourier transformation does not have to be transformed. The stresses can thus be expanded as

$$\hat{\boldsymbol{\sigma}}(k_x, k_y, z) = \frac{1}{2\pi} \sum_{j=1}^{6} a_j \boldsymbol{F}^{-1}\hat{\boldsymbol{D}}^{[j]}(k_x, k_y)\boldsymbol{\Psi}^{[j]}(k_x, k_y) e^{\mathrm{i}k_z^{[j]} z} \ , \tag{20}$$

where $\hat{\boldsymbol{D}}^{[j]}$ is a matrix representing the derivative operators in the Fourier do-

main at $k_z^{[j]}$ (see Eq. (43)), i.e.

$$\hat{\boldsymbol{D}}^{[j]}(k_x, k_y) = \hat{\boldsymbol{D}}(k_x, k_y, k_z^{[j]}) = \frac{1}{2}\begin{pmatrix} 2\mathrm{i}k_x & 0 & 0 \\ 0 & 2\mathrm{i}k_y & 0 \\ 0 & 0 & 2\mathrm{i}k_z^{[j]} \\ 0 & \mathrm{i}k_z^{[j]} & \mathrm{i}k_y \\ \mathrm{i}k_z^{[j]} & 0 & \mathrm{i}k_x \\ \mathrm{i}k_y & \mathrm{i}k_x & 0 \end{pmatrix}. \tag{21}$$

We assume that the layer has thickness d and define $(\hat{\boldsymbol{u}}_{\mathrm{top}}, \hat{\boldsymbol{\sigma}}_{\mathrm{top}})$ as the displacements and the stresses in the z direction (σ_{xz}, σ_{yz} and σ_{zz}, henceforth called z-stresses) on top, and $(\hat{\boldsymbol{u}}_{\mathrm{bot}}, \hat{\boldsymbol{\sigma}}_{\mathrm{bot}})$ as the displacements/z-stresses at the bottom of the layer. To enhance numerical stability, the origin of the local coordinate system is set to the middle of the layer. Furthermore we reorder the eigenpairs so that the first 3 eigenvalues have positive imaginary part. This is possible, because they are roots of a polynomial of degree 3 as a function of k_z^2. Additionally we define

$$\boldsymbol{\Psi} := (\boldsymbol{\Psi}^{[1]}, \boldsymbol{\Psi}^{[2]}, \boldsymbol{\Psi}^{[3]}) \ , \tag{22}$$

$$\boldsymbol{E}(z) := \mathrm{diag}(e^{\mathrm{i}k_z^{[1]}z}, e^{\mathrm{i}k_z^{[2]}z}, e^{\mathrm{i}k_z^{[3]}z}) \ , \tag{23}$$

$$\boldsymbol{a} := (a_1, \ldots, a_6)^T \ . \tag{24}$$

Using the special properties of the eigenpairs (namely that they come in pairs of $(k_z^{[j]}, \boldsymbol{\Psi}^{[j]})$ and $(-k_z^{[j]}, \boldsymbol{S}_3\boldsymbol{\Psi}^{[j]})$), the displacements and z-stresses on top and at the bottom of the layer are given as

$$\begin{pmatrix} \hat{\boldsymbol{u}}_{top} \\ \hat{\boldsymbol{u}}_{bot} \end{pmatrix} = \frac{1}{2\pi}\begin{pmatrix} \boldsymbol{\Psi}\boldsymbol{E}(-d/2) & \boldsymbol{S}_3\boldsymbol{\Psi}\boldsymbol{E}(-d/2)^{-1} \\ \boldsymbol{\Psi}\boldsymbol{E}(-d/2)^{-1} & \boldsymbol{S}_3\boldsymbol{\Psi}\boldsymbol{E}(-d/2) \end{pmatrix}\boldsymbol{a} \tag{25}$$

and

$$\begin{pmatrix} \hat{\boldsymbol{\sigma}}_{top} \\ \hat{\boldsymbol{\sigma}}_{bot} \end{pmatrix} = \frac{1}{2\pi}\begin{pmatrix} \mathring{\boldsymbol{\Psi}}\boldsymbol{E}(-d/2) & \boldsymbol{S}_3\mathring{\boldsymbol{\Psi}}\boldsymbol{E}(-d/2)^{-1} \\ \mathring{\boldsymbol{\Psi}}\boldsymbol{E}(-d/2)^{-1} & \boldsymbol{S}_3\mathring{\boldsymbol{\Psi}}\boldsymbol{E}(-d/2) \end{pmatrix}\boldsymbol{a} \ , \tag{26}$$

where $\mathring{\boldsymbol{\Psi}} := (\mathring{\boldsymbol{\Psi}}^{[1]}, \mathring{\boldsymbol{\Psi}}^{[2]}, \mathring{\boldsymbol{\Psi}}^{[3]})$, and $\mathring{\boldsymbol{\Psi}}^{[j]}$ contains those elements of $\boldsymbol{F}^{-1}\hat{\boldsymbol{D}}^{[j]}\boldsymbol{\Psi}$ that correspond to the z-stresses (please note that $\boldsymbol{E}(-d/2)^{-1} = \boldsymbol{E}(d/2)$ and that the positive z direction points downwards).

As a boundary condition on top of the soil (at $z = 0$), the z-stresses are set to 0 to reflect the free surface. For $z \to +\infty$ (i.e. in the half space), a Sommerfeld like radiation condition needs to be fulfilled, i.e. $\hat{\boldsymbol{u}} \to 0$ (and consequently $\hat{\boldsymbol{\sigma}} \to 0$) as $z \to +\infty$, thus $a_4 = a_5 = a_6 = 0$, because of the way the eigenvalues are ordered (see the exponential term in Eq. (20)).

4.2 Multiple layers

Once a formulation for one single layer is found, the expansion to multiple layers is straight forward. Let $\hat{\boldsymbol{u}}^I_{\mathrm{bot}}$, $\hat{\boldsymbol{\sigma}}^I_{\mathrm{bot}}$ be the displacements and stresses at the bottom of a layer, and $\hat{\boldsymbol{u}}^{II}_{\mathrm{top}}$, $\hat{\boldsymbol{\sigma}}^{II}_{\mathrm{top}}$ the displacements and stresses at the top of the layer underneath. $\hat{\boldsymbol{p}}$ is a (possible) load vector on top of the second layer, that points either in the x, y or z direction. With the assumption of free wave

propagation, loads may only be applied at layer boundaries using boundary conditions.

The two layers can be connected (including the boundary conditions) using

$$\begin{pmatrix} \hat{\boldsymbol{u}}^{II}_{\text{top}} \\ \hat{\boldsymbol{\sigma}}^{II}_{\text{top}} \end{pmatrix} = \begin{pmatrix} \hat{\boldsymbol{u}}^{I}_{\text{bot}} \\ \hat{\boldsymbol{\sigma}}^{I}_{\text{bot}} \end{pmatrix} - \begin{pmatrix} 0 \\ \hat{\boldsymbol{p}} \end{pmatrix} . \tag{27}$$

We have seen in Section 3, that in our approach it will be necessary to also apply loads at collocation nodes (y_p, z_p) inside a (material) layer. In that case the layer is split into two virtual layers (i.e. two adjacent layers with the same material properties) at the load depth. Because of the shift invariance of the fundamental solutions, it is only necessary to apply the load at the origin $(0, 0)$ of the horizontal plane at each depth z_p (see also Eq. (4)).

Combining Eqs. (25), (26) and (27), a global linear system can be derived:

$$\mathbf{M}\hat{\mathbf{u}}_{\text{global}} = \hat{\mathbf{p}}_{\text{global}} , \tag{28}$$

where $\hat{\mathbf{p}}_{\text{global}}$ is defined by a point load at an arbitrary load point $\boldsymbol{\xi}$ in some depth z_p, and $\hat{\mathbf{u}}_{\text{global}}$ is the vector of displacements at the different layer boundaries.

Note that once Eq. (28) is solved, the unknown coefficients $\boldsymbol{a}$ in Eq. (25) can easily be calculated, an thus the fundamental z-stresses and displacements at an arbitrary depth. Also note that $\hat{\boldsymbol{u}}$ and $\hat{\boldsymbol{\sigma}}$ are still functions of (k_x, k_y, z).

5 Numerical Evaluation of the Integrals

In general, the integrands in Eq. (2) become singular as $\boldsymbol{\xi} \to \boldsymbol{x}$. With the Fourier transformation this 'locally improper' integral (meaning an integral over a bounded domain, but with an unbounded integrand) becomes a 'globally improper' integral (an integral over an unbounded domain with a bounded integrand).

If load and evaluation point have the same depth, the stresses and therefore the integrands are non-decaying as $k_y \to \pm\infty$, which is a serious problem for a numerical inverse Fourier transformation.

Both kinds of 'improperness' ('local' and 'global' one) can be avoided by solving the BIE in the semi-Fourier domain (k_x, k_y, z) (i.e. using the fundamental solution in the form that was discussed in Section 4) and postponing the inverse Fourier transformation until the evaluation of the boundary integral has been completed.

5.1 Single layer potential

First we take a look at the right hand side of Eq. (8), given by Eq. (11):

$$\mathbf{f}_p = \left(\int_{\Gamma'_q} \breve{\boldsymbol{U}}^*(y_p, z_p; y, z) \; d\Gamma'_q \right) \breve{\boldsymbol{t}}(y_q, z_q) , \tag{29}$$

where any dependencies on k_x have been omitted, because of the reduction to 2.5D (see Section 3.1). At the surface of the tunnel we assume the Neumann like boundary conditions $\breve{\boldsymbol{t}}(y_q, z_q) = \mathbf{0}$ for all points on Γ', except at the tunnel base in the depth z_{base}, where the external load is applied between y_{left} and y_{right}.

This load is modeled using the boundary conditions $\breve{t}_z(y, z_{\text{base}}) = f$, where f is the constant strength of the applied load in the z direction. Therefore, the integral in Eq. (29) over a single horizontal element is

$$f \cdot \int_{-y_0}^{y_0} \breve{u}^*_{iz}(y_p, z_p; y + y_q, z_{\text{base}})\ dy\ , \tag{30}$$

where (y_q, z_{base}) and $2y_0$ are reference point and length of the element Γ'_q respectively (see Fig. 2).

Using shift invariance with respect to the horizontal direction y (see Eqs. (41) and (4)), applying the Fourier transformation in the same direction (cf. Eq. (45)), and finally exchanging the order of integration, yields

$$\begin{aligned} f \int_{-y_0}^{y_0} \breve{u}^*_{iz}(0, z_p; y + y_q - y_p, z_{\text{base}})\ dy = \\ \frac{1}{2\pi} f \int_{-y_0}^{y_0} \int_{-\infty}^{\infty} e^{-\mathrm{i}k_y(y_q - y_p)} \hat{u}^*_{iz}(0, z_p; k_y, z_{\text{base}}) e^{-ik_y y}\ dk_y\ dy = \\ \frac{1}{2\pi} f \int_{-\infty}^{\infty} e^{-\mathrm{i}k_y(y_p - y_q)} \hat{u}^*_{iz}(0, z_p; k_y, z_{\text{base}}) \int_{-y_0}^{y_0} e^{-\mathrm{i}k_y y}\ dy\ dk_y\ . \end{aligned} \tag{31}$$

The last integral can be calculated analytically ($\int_{-b}^{b} e^{-\mathrm{i}ax}\ dx = 2b\ \mathrm{sinc}(ab)$, where $\mathrm{sinc}(x) := \frac{\sin(x)}{x}$), thus Eq. (31) becomes:

$$\frac{1}{\pi} f y_0 \int_{-\infty}^{\infty} e^{-ik_y(y_p - y_q)} \hat{u}^*_{iz}(0, z_p; k_y, z_{\text{base}})\ \mathrm{sinc}(k_y y_0)\ dk_y\ . \tag{32}$$

The displacements $\hat{u}^*_{iz}(k_y)$ are bounded and the sinc-function ensures the decay of the integrand as $k_y \to \pm\infty$, which makes it possible to calculate the integral numerically using simple quadrature schemes. Note that, due to its purely imaginary exponent, also the exponential term is bounded.

5.2 Double layer potential

For the numerical solution of the integral in Eq. (9), we look at the ij-th entry of the matrix block $\mathbf{M}_{pq}$:

$$\frac{1}{2}\delta_{pq}\delta_{ij} + \int_{\Gamma'_q} \breve{t}^*_{ij}(y_p, z_p; y, z)\ d\Gamma'_q\ . \tag{33}$$

Using Eq. (3), the integral in this equation can be reduced to

$$\sum_{k=1}^{3} n_k(y_q, z_q) \int_{\Gamma'_q} \breve{\sigma}^*_{ijk}(y_p, z_p, y, z)\ d\Gamma'_q\ , \tag{34}$$

where $\breve{\sigma}^*_{ijk}$ is given by the fundamental stresses constructed in Section 4, i.e. $\breve{\sigma}^*_{ijk}$ is the stress tensor $\breve{\sigma}_{jk}$ at the point $(y, z) \in \Gamma'_q$ caused by a point load in the i direction at point (y_p, z_p).

Because every element of the discretization of Γ' belongs to two virtual layers (the collocation point is the midpoint), it has to be split into two parts for the integration. Since both parts are straight lines, they can be parameterized by

$(y,z)^T = (y_{q'} - \cos(\alpha)s, z_{q'} + \sin(\alpha)s)^T,\ s \in [-b,b]$, where $2b$ is the length of the part of the element, α its inclination (cf. Fig.(2)) and $(y_{q'}, z_{q'})$ is the midpoint of the respective part of the element $\Gamma_{q'}$. Following the same idea as in the case of the single layer potential, we exchange inverse Fourier transformation and integration over the element, thus the integral in Eq. (34) for one part of the element is given as

$$\int_{\Gamma'_{q'}} \breve{\sigma}^*_{ijk}(0, z_p; y - y_p, z)\ d\Gamma'_{q'} =$$

$$\int_{-b}^{b} \breve{\sigma}^*_{ijk}(0, z_p; y_{q'} - \cos(\alpha)s - y_p, z_{q'} + \sin(\alpha)s)\ d\Gamma'_{q'} =$$

$$\frac{1}{2\pi} \int_{-\infty}^{\infty} e^{-\mathrm{i}k_y(y_p - y_{q'})} \int_{-b}^{b} \hat{\sigma}^*_{ijk}(0, z_p; k_y, z_{q'} + \sin(\alpha)s) e^{-\mathrm{i}k_y \cos(\alpha)s}\ ds\ dk_y\ . \quad (35)$$

By construction (cf. Eq. (20)) the entries of $\hat{\sigma}^*_{ijk}$ are given as linear combinations of exponential functions in z and matrices whose components only dependent on k_y (and k_x, which is omitted here):

$$\hat{\sigma}^*_{ijk}(0, z_p; k_y, z_q + \sin(\alpha)s) =$$

$$\sum_{\ell=1}^{6} a^{[\ell]}(i, z_p) \hat{\Phi}^{[\ell]}_{jk}(k_y) e^{\mathrm{i}k_z^{[\ell]}(z_q + \sin(\alpha)s)}\ , \quad (36)$$

where the coefficients $a^{[\ell]}$ depend on the load applied at the depth z_p and its direction i and the $\hat{\Phi}^{[\ell]}_{jk}$ are the components of $\boldsymbol{F}^{-1}\hat{\boldsymbol{D}}^{[\ell]}\boldsymbol{\Psi}^{[\ell]}$ properly reordered into matrix form.

Combining Eqs. (35) and (36) we get for the integral over s:

$$\sum_{\ell=1}^{6} a^{[\ell]}(i, z_p) \hat{\Phi}^{[\ell]}_{jk}(k_y) e^{\mathrm{i}k_z^{[\ell]} z_q} \int_{-b}^{b} e^{-\mathrm{i}s(k_y \cos(\alpha) - k_z^{[\ell]} \sin(\alpha))}\ ds\ . \quad (37)$$

We see that the integral with respect to s only contains exponential functions, thus it can again be calculated analytically. The result of this integration is once more a sinc-function, which provides damping and leads to a decay with respect to k_y of the integrand, that is suitable for numerical integration of the final expression:

$$\frac{1}{\pi} b \int_{-\infty}^{\infty} e^{-\mathrm{i}k_y(y_p - y_{q'})} \sum_{\ell=1}^{6} a^{[\ell]}(i, z_p) \hat{\Phi}^{[\ell]}_{jk}(k_y) e^{\mathrm{i}k_z^{[\ell]} z_q}\ \cdot$$

$$\cdot\ \mathrm{sinc}(b(k_y \cos(\alpha) - k_z^{[\ell]} \sin(\alpha)))\ dk_y\ . \quad (38)$$

The advantages of our method over a model that applies the inverse Fourier transformation at an earlier stage are, that in our approach the integration over the boundary elements can be done analytically. The additional sinc-term stemming from this integration dampens the integrand as $k_y \to \pm\infty$, leading to a smaller domain for the numerical integration.

Layer 1:	$E_x = E_z = 9.000 \cdot 10^7 + 3.600 \cdot 10^6 \mathrm{i}$,	$\nu_x = \nu_{zx} = 0.330$
	$G_{zx} = 3.375 \cdot 10^7 + 1.350 \cdot 10^6 \mathrm{i}$,	$\rho = 1500$, $d = 7.0$
Layer 2:	$E_x = E_z = 3.110 \cdot 10^8 + 1.244 \cdot 10^7 \mathrm{i}$,	$\nu_x = \nu_{zx} = 0.314$
	$G_{zx} = 1.183 \cdot 10^8 + 4.732 \cdot 10^6 \mathrm{i}$,	$\rho = 1750$, $d = 2.0$
Layer 3:	$E_x = E_z = 9.000 \cdot 10^7 + 3.600 \cdot 10^6 \mathrm{i}$,	$\nu_x = \nu_{zx} = 0.330$
	$G_{zx} = 3.375 \cdot 10^7 + 1.350 \cdot 10^6 \mathrm{i}$,	$\rho = 1500$, $d = 5.0$
Half space:	$E_x = E_z = 3.555 \cdot 10^8 + 1.421 \cdot 10^7 \mathrm{i}$,	$\nu_x = \nu_{zx} = 0.315$
	$G_{zx} = 1.352 \cdot 10^8 + 5.408 \cdot 10^6 \mathrm{i}$,	$\rho = 2000$

Table 1: Material parameters for the test problem in SI-units.

6 Implementation

Our implementation was done in Fortran using LAPACK subroutines. It is part of a software package that was successfully used in earlier projects [37].

6.1 Example

As a test problem for our algorithm, we chose a tunnel whose cross section is a circle with a radius of 3 m. Its center is positioned 9 m below surface. 1.5 m below the center, the circle is cut by a horizontal line, thus giving the tunnel a horizontal floor. This cross section was discretized with 101 straight elements with lengths ranging from 0.10 m to 0.18 m.

The soil consist of three isotropic layers of different thickness, additionally a half space layer was added to prevent unwanted reflections. For the parameters see Tab. 1. A pressure load of 10 N/m^2 was applied at $x = 0$ and $y \in [-2, 2]$ at the tunnel base pointing in the z direction. The discretization of the (k_x, k_y)-plane was done with an equidistant grid in $[-5, 5] \times [-5, 5]$ with 200 points per direction. This restriction to a finite square of the (k_x, k_y)-plane corresponds to a periodization of the setting [38, 39]. All calculations were made for a frequency of 40 Hz.

Fig. 3 shows the real part of the displacements in the z direction at the tunnel wall and base, and the surface.

6.2 Influence of the Fourier Grid

Fig. 4 shows the dependence of the accuracy of the solution on the discretization in the Fourier domain. The result for six equidistant discretizations of the same section of the Fourier domain $(k_x, k_y) = [-5, 5] \times [-5, 5]$ are shown. In the studied example, using more than 128 grid points does not significantly increase the accuracy.

Regarding efficiency, the method proposed here is remarkable in the sense that it needs very little memory, since only small matrices have to be kept in the memory. This is due to the facts that the calculations for every frequency and every wavenumber can be done separately.

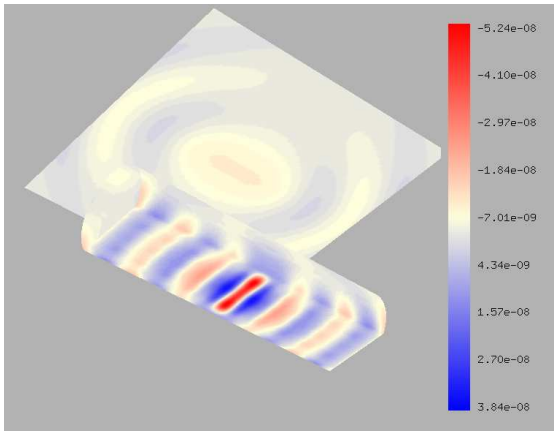

Figure 3: Real part of the displacements of the tunnel wall and base, and the surface in the z direction at 40 Hz. A pressure load of 10 N/m^2 was applied at $x = 0$ and $y \in [-2, 2]$ at the tunnel base pointing in the z direction. The deformations are in meters.

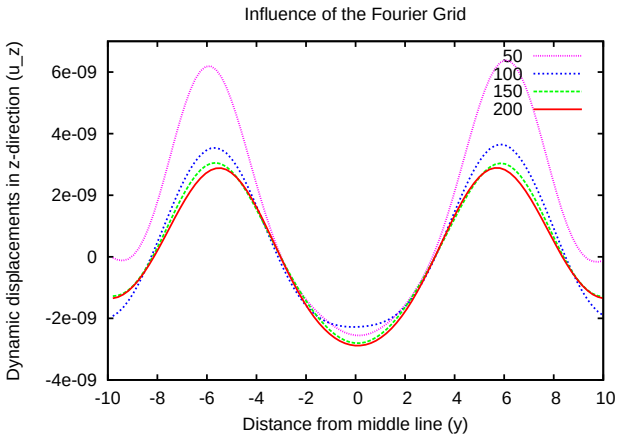

Figure 4: Dependence on the discretization in the Fourier domain. The figure shows the real part of the dynamic displacements in the z direction at 40 Hz at the surface along a line perpendicular to the tunnel and 10 m from the centre $u_z(x = \pm 10, y, z = 0)$. The result is displayed for different discretizations of the same section of the Fourier domain, $(k_x, k_y) = [-5, 5] \times [-5, 5]$, with equidistant grids with 50×50 to 200×200 points. Refining the grid further did not change the result significantly. All other parameters are as in the test problem in Sec. 6.1. The deformations and distances are in meters.

6.3 Influence of Anisotropy

Fig. 5 shows the influence of anisotropy on the solution. It can be seen that material parameters that differ slightly from the isotropic case, can have significant effects on the vibration at the surface.

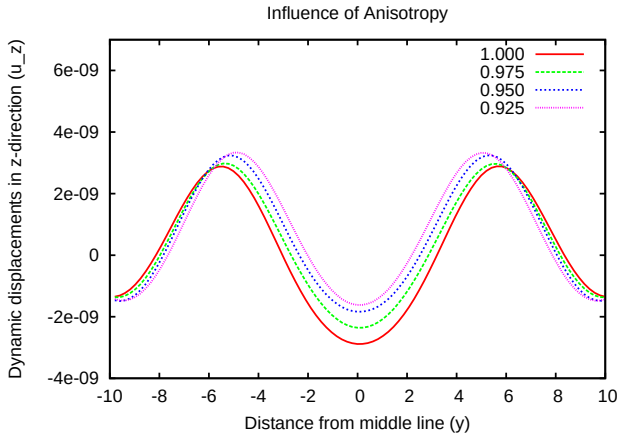

Figure 5: Influence of anisotropy. The figure shows the real part of the displacements in the z direction at 40 Hz at the surface along a line perpendicular to the tunnel and 10 m from the centre $u_z(x = \pm 10, y, z = 0)$. The numbers in the legend indicate the ratio between the real parts of E_x and E_z, and G_{zx} and G_{xy} respectively for the uppermost layer. All other parameters are as in the test problem in Sec. 6.1. The deformations and distances are in meters.

6.4 Comparison with other methods

In [12], Gupta et al. used a soil model consisting of four material layers on top of a half space. To test our soil model, we adapted their material parameters (rounded values given in [12, Tab. 1]) to fit our input format. The parameters used are given in Tab. 2.

We apply a load in z-direction at a depth of 29.5m and look at the real part of the horizontal and vertical component of $\breve{\boldsymbol{u}}^*(y, z)$ for a frequency of 40 Hz. The result is depicted in Fig. 6. There seems to be good agreement with the results from [12, Fig. 10 b], except for some differences in the upper layer, which might be caused by slight numerical differences in the material parameters.

7 Conclusions and Outlook

A boundary element model to calculate displacements in soil consisting of layers of anisotropic media caused by a vibrating load inside a tunnel was presented. An approximation for the fundamental displacements and stresses was calculated numerically in the Fourier domain. This result was then used to set up the BIE. It was shown that the BIE can be decoupled for every wave number k_x, giving a natural way to apply parallel computation. It was pointed out that

Layer 1:	$E_x = E_z = 8.300 \cdot 10^6 + 2.075 \cdot 10^5$i, $G_{zx} = 2.7675 \cdot 10^6 + 6.9188 \cdot 10^4$i,	$\nu_x = \nu_{zx} = 0.4996$ $\rho = 1107$, $d = 3.7$
Layer 2:	$E_x = E_z = 2.5296 \cdot 10^7 + 6.324 \cdot 10^6$i , $G_{zx} = 8.4375 \cdot 10^6 + 2.1094 \cdot 10^5$i,	$\nu_x = \nu_{zx} = 0.4990$ $\rho = 1500$, $d = 7.0$
Layer 3:	$E_x = E_z = 1.9074 \cdot 10^8 + 4.7686 \cdot 10^6$i, $G_{zx} = 6.3828 \cdot 10^7 + 1.5957 \cdot 10^6$i,	$\nu_x = \nu_{zx} = 0.4942$ $\rho = 1970$, $d = 8.3$
Layer 4:	$E_x = E_z = 3.3815 \cdot 10^8 + 8.4537 \cdot 10^6$i, $G_{zx} = 1.1347 \cdot 10^8 + 2.8368 \cdot 10^6$i,	$\nu_x = \nu_{zx} = 0.4900$ $\rho = 1970$, $d = 9.3$
Half space:	$E_x = E_z = 3.9643 \cdot 10^8 + 8.4537 \cdot 10^6$i, $G_{zx} = 1.312 \cdot 10^8 + 2.3279 \cdot 10^6$i,	$\nu_x = \nu_{zx} = 0.4884$ $\rho = 1970$

Table 2: Material parameters for the comparison to the results in [12] in *SI*-units.

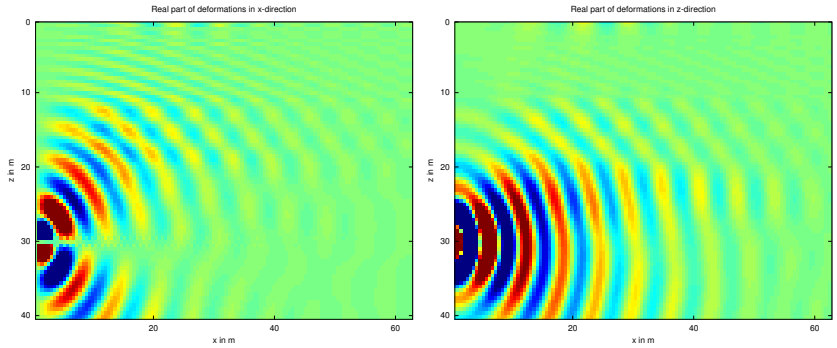

Figure 6: The horizontal (left) and vertical component (right) of the dynamic deformations in a layered half space without a tunnel for a harmonic point load applied at a depth of 29.5 m at 40 Hz. Material parameters were chosen as close as possible to [12, Tab. 1].

exchanging the integrals over k_y for the inverse Fourier transformation and the one over the boundary element makes it possible to solve the latter analytically. Thus only one of the two integrals has to be calculated numerically. Furthermore our method also leads to a better decay of the integrand for the integration over the unbounded k_y-domain.

Another advantage of this change in order of integration is, that one can use equidistant grids in both, the Fourier- and the time-domain, because it is not necessary to use a very fine grid around the singularities of the integrand.

The focus of future work will be on exploiting properties of the fundamental solutions. As the fundamental solutions get very smooth for large k_x and k_y, this certainly should have some influence on the wavenumber grid, where the fundamental solution is calculated. Additionally it will be investigated, how the asymptotic behavior of the eigenpairs can be used to improve the method. Efforts have also been made to merge virtual layers into one material layer again, giving the advantage that the system of equations to calculate an approximation of the fundamental solutions can be kept significantly smaller.

Acknowledgement

This work was supported by the Austrian Federal Ministry of Transport, Innovation and Technology under the grant Bmvit-isb2 and the FFG under the project Pr. Nr. 809089.

A Notation and basic Definitions

Here we give some notation and basic definitions. The Fourier transform of a function $g(t)$ with respect to its variable t (the result of the application of the Fourier transformation $\mathcal{F}_t$) is defined as

$$\mathcal{F}_t[g(t)] = [\mathcal{F}_t g](\nu) = \int_{-\infty}^{\infty} g(t) e^{-\mathrm{i}t\nu} \, dt \ , \tag{39}$$

whereas its inverse is

$$(\mathcal{F}_t)^{-1}[h(\nu)] = [(\mathcal{F}_t)^{-1} h](t) = \frac{1}{2\pi} \int_{-\infty}^{\infty} h(\nu) e^{\mathrm{i}t\nu} \, d\nu \ . \tag{40}$$

Some important properties of the Fourier transformation, that will be used in this article, are:

$$\mathcal{F}_t[g(t-\tau)] = e^{-\mathrm{i}\tau\nu} \mathcal{F}_t[g(t)] = e^{-\mathrm{i}\tau\nu} [\mathcal{F}_t g](\nu) \ , \tag{41}$$

$$\mathcal{F}_t \left[\int_{-\infty}^{\infty} g(\tau - t) h(\tau) \, d\tau \right] = [\mathcal{F}_t g](-\nu) \cdot [\mathcal{F}_t h](\nu) \text{ and} \tag{42}$$

$$\mathcal{F}_t \left[\frac{d}{dt} g(t) \right] = \mathrm{i}\nu \ \mathcal{F}_t[g(t)] = \mathrm{i}\nu \ [\mathcal{F}_t g](\nu) \ . \tag{43}$$

Since we will 'switch around' between several domains, we here introduce certain superscripts for the symbol of a function in the regular domain $u(x, y, z)$.

We use the tilde ($\tilde{\cdot}$) to denote entities in the (k_x, k_y, k_z)-domain, the hat ($\hat{\cdot}$) indicates functions in the (k_x, k_y, z)-domain, and the breve ($\breve{\cdot}$) is related to the (k_x, y, z)-domain. With this notation we can readily identify the various transforms of a function and their respective domains:

$$\mathcal{F}_x[u(x,y.z)] = [\mathcal{F}_x u](k_x,\ y,\ z) = \breve{u}(k_x,\ y,\ z)\ , \tag{44}$$

$$\mathcal{F}_y[\mathcal{F}_x[u(x,y,z)]] = \mathcal{F}_y[\breve{u}(k_x,y,z)] = [\mathcal{F}_y \breve{u}](k_x,k_y,\ z) = \hat{u}(k_x,k_y,\ z)\ , \tag{45}$$

$$\mathcal{F}_z[\mathcal{F}_y[\mathcal{F}_x[u(x,y,z)]]] = [\mathcal{F}_z \hat{u}](k_x,k_y,k_z) = \tilde{u}(k_x,k_y,k_z)\ . \tag{46}$$

The two- and three-dimensional Fourier transformations are simply compositions of the one-dimensional transformation, performed with respect to mutually independent variables (corresponding to different spatial directions).

Furthermore, the asterisk ($\cdot^*$) denotes the fundamental solution.

B Entries of matrix $\boldsymbol{A}$

$$\begin{aligned}
A_{11} &= \frac{(E_z - \nu_{zx}^2 E_x)E_x k_x^2}{(\nu_{xy}^2 - 1)E_z + 2(1+\nu_{xy})\nu_{zx}^2 E_x} - G_{xy}k_y^2 - G_{xy}k_z^2 + \rho\omega^2 \\
A_{12} = A_{21} &= \frac{(\nu_{xy}E_z + \nu_{zx}^2 E_x)E_x k_x k_y}{(\nu_{xy}^2 - 1)E_z + 2(1+\nu_{xy})\nu_{zx}^2 E_x} - G_{xy}k_x k_y \\
A_{13} = A_{31} &= \frac{\nu_{zx}E_z E_x k_x k_z}{(\nu_{xy} - 1)E_z + 2\nu_{zx}^2 E_x} - G_{zx}k_x k_z \\
A_{22} &= \frac{(E_z - \nu_{zx}^2 E_x)E_x k_y^2}{(\nu_{xy}^2 - 1)E_z + 2(1+\nu_{xy})\nu_{zx}^2 E_x} - G_{xy}k_x^2 - G_{xy}k_z^2 + \rho\omega^2 \\
A_{23} = A_{32} &= \frac{\nu_{zx}E_z E_x k_y k_z}{(\nu_{xy} - 1)E_z + 2\nu_{zx}^2 E_x} - G_{zx}k_y k_z \\
A_{33} &= \frac{(\nu_{zx} - 1)E_z^2 k_z^2}{(\nu_{xy}^2 - 1)E_z + 2\nu_{zx}^2 E_x} - G_{zx}(k_x^2 + k_y^2) + \rho\omega^2
\end{aligned}$$

References

[1] P. Moczo, J. Kriszek, E. Bystický, Efficiency and optimization of the 3-D finite-difference modeling of seismic ground motion, J. Comput. Acoust. 9 (2) (2001) 593–609.

[2] M. Tadi, Finite difference methods for elastic wave propagation in layered media, J. Comput. Acoust. 12 (2) (2004) 257–276.

[3] P. Balazs, W. Kreuzer, H. Waubke, A stochastic 2D-model for calculating vibrations in random layers, J. Comput. Acoust. 15 (3) (2007) 271–283.

[4] W. Kreuzer, H. Waubke, G. Rieckh, P. Balazs, A 3D model to simulate vibrations in a layered medium with stochastic material parameters, J. Comput. Acoust. 19 (2011) 139–154.

[5] P. Galvin, J. Dominguez, Analysis of ground motion due to moving surface loads induced by high-speed trains, Eng. Anal. Bound. Elem. 31 (11) (2007) 931–941.

[6] M. Sari, I. Demir, Wave Modelling Through Layered Media Using BEM, J. Appl. Sci. 6 (8) (2006) 1703–1711.

[7] A. J. B. Tadeu, E. Kausel, C. Vrettos, Scattering of waves by subterranean structures via the boundary element method, Soil Dyn. Earthq. Eng. 15 (6) (1996) 387–397.

[8] H. Waubke, Boundary Element Method for Isotropic Media with Random Shear Moduli, J. Comput. Acoust. 13 (1) (2005) 229–258.

[9] X. Sheng, C. Jones, D. Thompson, Modelling ground vibration from railways using wavenumber finite- and boundary element methods, Proc. R. Soc. A 461 (2005) 2043–2070.

[10] L. Andersen, C. Jones, Vibration from a Railway Tunnel Predicted by Coupled Finite Element and Boundary Element Analysis in Two and Three Dimensions, in: H. Grundmann, G. I. Schuëller (Eds.), Structural Dynamics, Eurodyn 2002, Vol. 2, Swets & Zeitlinger B.B., Lisse, The Netherlands, 2002, pp. 1131–1136.

[11] S. Gupta, M. Hussein, G. Degrande, H. Hunt, D. Clouteau, A comparison of two numerical models for the prediction of vibrations from underground railway traffic, Soil Dyn. Earthq. Eng. 27 (7) (2007) 608–624.

[12] S. Gupta, H. V. den Berghe, G. Lombaert, G. Degrande, Numerical modelling of vibrations from a Thalys high speed train in the Groene Hart tunnel, Soil Dyn. Earthq. Eng. 30 (3) (2010) 82–97.

[13] P. Jean, Boundary and Finite Elements for 2D Soil-Structure Interaction Problems, Acta Acust. & Acustica 87 (1) (2001) 56–66.

[14] L. Gaul, M. Kögl, M. Wagner, Boundary Element Methods for Engineers and Scientists, An Introductory Course with Advanced Topics, Springer, Berlin Heidelberg, 2003.

[15] J. Liao, C. Wang, Elastic solutions for a transversely isotropic half-space subjected to a point load, Int. J. Numer. Anal. Met. 22 (6) (1998) 425–447.

[16] I. V. Boykov, A. I. Boykova, E. S. Ventsel, Fundamental solutions for thick sandwich plates, Eng. Anal. Bound. Elem. 28 (2004) 1437–1444.

[17] M. Eskandari-Ghadi, S. Sture, R. Pak, A. Ardeshir-Behrestaghi, A trimaterial elastodynamic solution for a transversely isotropic full-space, Int. J. Solids Struct. 46 (5) (2009) 1121–1133.

[18] E. Kausel, Dynamic point sources in laminated media via the thin-layer method, Int. J. Solids Struct. 36 (31–32) (1999) 4725–4742.

[19] E. Pan, F. Han, Green's functions for transversely isotropic piezoelectric functionally graded multilayered half spaces, Int. J. Solids Struct. 42 (11-12) (2005) 3207–3233.

[20] A. J. B. Tadeu, E. Kausel, Greens functions for two-and-a-half-dimensional elastodynamic problems, J. Eng. Mech. 126 (2000) 1093–1097.

[21] A. Tadeu, J. Antonio, 2.5D Greens Functions for Elastodynamic Problems in Layered Acoustic and Elastic Formations, CMES – J. Comput Model. Engng. Sci. 2 (4) (2001) 477–495.

[22] H. Schmidt, G. Tango, Efficient global matrix approach to the computation of synthetic seismograms, Geophys. J. Royal Astron. Soc. 84 (1986) 331–359.

[23] J. Wideberg, F. Benitez, Elastic stress and displacement distribution in an orthotropic multilayered system due to a concentrated load, Eng. Anal. Bound. Elem. 16 (1) (1995) 19–27.

[24] J. Xu, T. Davies, E. Pan, Efficient and accurate multi-layered elastostatic Green's functions via the bi-material Green's function, Eng. Anal. Bound. Elem. 31 (8) (2007) 683–691.

[25] B. Yang, E. Pan, Efficient evaluation of three-dimensional Green's functions in anisotropic elastostatic multilayered composites, Eng. Anal. Bound. Elem. 26 (4) (2002) 355–366.

[26] F. Yuan, S. Yang, B. Yang, Three-dimensional Green's functions for composite laminates, Int. J. Solids Struct. 40 (2) (2003) 331–342.

[27] F. Duddeck, Fourier-BEM: or what to do if no fundamental solution is available?, Meccanica 36 (2001) 437–448.

[28] P. Jean, C. Guigou, M. Villot, A 2.5D BEM Model for Ground-Structure Interaction, Build. Acoust. 11 (3) (2004) 157–173.

[29] J. Lu, D. Jeng, S. Williams, A 2.5-D dynamic model for a saturated porous medium. part II: Boundary element method, Int. J. Solids Struct. 45 (2) (2008) 359–377.

[30] K. Müller, H. Grundmann, S. Lenz, Nonlinear interaction between a moving vehicle and a plate elastically mounted on a tunnel, J. Sound Vib. 310 (2008) 558–586.

[31] S. François, M. Schevenels, P. Galvin, G. Lombaert, G. Degrande, A 2.5D coupled FE-BE methodology for the dynamic interaction between longitudinally invariant structures and a layered halfspace, Comput. Methods Appl. Mech. Engrg. 199 (2010) 1536–1548.

[32] A. Tadeu, A. Pereira, L. Godinho, J. Antonio, Prediction of airborne sound and impact sound insulation provided by single and multilayer systems using analytical expressions, Appl. Acoust. 68 (1) (2007) 17–42.

[33] G. Rieckh, H. Waubke, W. Kreuzer, Vibrations in layered anisotropic soil: 2.5D-Fourier-BEM and parallel computation, in: Proceedings of the 8th International Conference on Structural Dynamics, EURODYN 2011, Leuven, Belgium, 2011, pp. 570–573.

[34] H. Waubke, Dynamische Berechnungen für den Halbraum mit streuenden Parametern mittels orthogonaler Polynome, Tech. rep., Technische Universität München (1996).

[35] F. Hartmann, Methode der Randelemente, Boundary Elements in der Mechanik auf dem PC, Springer, Berlin Heidelberg, 1987.

[36] F. Tisseur, K. Meerbergen, The quadratic eigenvalue problem, SIAM Rev. 43 (2001) 235–286.

[37] H. Waubke, Prognose der Erschütterungsausbreitung entlang von Bahn- und Tunnelstrecken, Tech. Rep. TM-10-2005-1, Institut für Schallforschung, Österreichische Akademie der Wissenschaften (2005).

[38] N. Kaiblinger, Approximation of the Fourier Transform and the Dual Gabor Window, J. Fourier Anal. Appl. 11 (2005) 25–42.

[39] P. L. Søndergaard, Gabor frames by sampling and periodization, Adv. Comput. Math. 27 (4) (2007) 355–373.